Paper II

II

Short reflectors operating at the fundamental and second harmonics on 128° $LiNbO_3$

S. Lehtonen, V. P. Plessky, and M. M. Salomaa

S. Lehtonen, V. P. Plessky, and M. M. Salomaa, "Short reflectors operating at the fundamental and second harmonics on 128° $LiNbO_3$", IEEE Transactions on Ultrasonics, Ferroelectrics, and Frequency Control, Vol. 51, No. 3, March 2004, pp. 343-351.

Short Reflectors Operating at the Fundamental and Second Harmonics on 128° $LiNbO_3$

Saku Lehtonen, Victor P. Plessky, *Senior Member, IEEE*, and Martti M. Salomaa, *Member, IEEE*

***Abstract*—In this work, we study numerically the operation of surface acoustic wave (SAW) reflectors comprising a small number of electrodes on the 128° YX-cut lithium niobate ($LiNbO_3$) substrate. The electrodes have a finite thickness, and they are either open circuited or grounded. The center-to-center distance between adjacent electrodes d corresponds roughly either to half of the characteristic wavelength $d \propto \lambda_0/2$ or to $d \propto \lambda_0$, for the reflectors operating at the fundamental and second harmonic modes, respectively. We use software based on the finite-element and boundary-element methods (FEM/BEM) for numerical experiments with a tailored test structure having 3 interdigital transducers (IDTs), simulating experimental conditions with an incident wave and reflected and transmitted SAWs. Using the fast Fourier transform (FFT) and time-gating techniques, calculation of the Y-parameters in a wide frequency range with rather a small step allows us to determine the reflection coefficients, and to estimate the energy loss due to bulk-wave scattering. The detailed dependences of the attenuation and reflectivity on the metallization ratio and the electrode thickness are given for the classic 128°-cut of $LiNbO_3$.**

I. Introduction

It is well-known [1] that, in strong piezoelectrics, very short reflectors comprising a small number of electrodes exhibit a behavior different from that of a periodic array of electrodes because the charge distributions on the electrodes can be different in the two cases. Moreover, the properties of the reflector depend on the termination conditions (open circuit or termination to ground). The energy losses due to the waves scattered into the bulk are also strongly dependent on the frequency and different for open and short-circuited electrodes [1].

For electrodes of finite thickness, such data is practically absent. In certain applications, such as SAW tags, relatively weak reflectors consisting of a few electrodes are used. In some cases, several reflectors can be put into the same acoustic channel [2], [3], and the tight control of reflectivity, parasitic multiple reflections, and losses are of primary importance.

In this work we study reflectors comprising 1-3 electrodes (different thicknesses of the aluminium electrodes and metallization ratios are considered) operating both at the fundamental frequency, when the center-to-center distance between the adjacent fingers d is commeasurable with half the SAW wavelength $\lambda_0/2$ or, at the second harmonic, with d close to λ_0. Preliminary results of this work were reported in [4].

Manuscript received June 19, 2002; accepted October 20, 2003.

S. Lehtonen and M. M. Salomaa are with the Materials Physics Laboratory, Helsinki University of Technology, FIN-02015 HUT, Finland (e-mail: saku@focus.hut.fi).

V. P. Plessky is with GVR Trade SA, CH-2022 Bevaix, Switzerland.

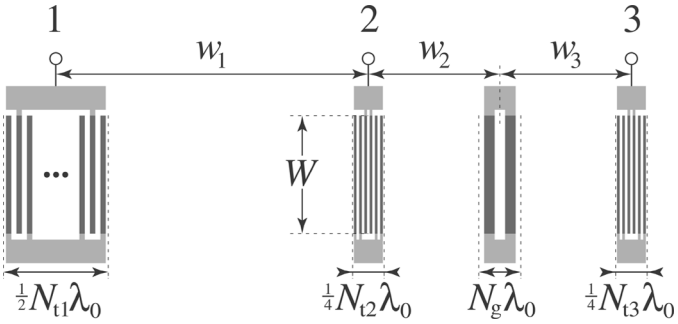

Fig. 1. Test structure for simulations of short reflectors on 128° $LiNbO_3$. The values $N_{t1} = 21$, $N_{t2} = N_{t3} = 6$, $N_g = 1 \ldots 3$, $\lambda_0 = 1.6$ μm, $W = 200$ μm, $w_1 = 160$ μm, and $w_2 = w_3 = 64$ μm are used.

This paper is organized as follows. In Section II we discuss the test structure used for numeric experiments. In Section III we describe the procedures used to extract the parameters for reflectivity and energy loss. Section IV presents the results for different reflector geometries and load conditions. Section V summarizes our results.

II. Test Structure

To study the characteristics of short reflectors, we conducted a numerical experiment with a tailored test structure, similar to the one used earlier for long reflectors [5]. The test structure (Fig. 1) includes a rather long and efficient input transducer (electrical port 1), two identical, split-finger receiving transducers with only a few electrodes (ports 2 and 3), and the device under test, the reflector, placed between the receiving transducers. The center-to-center distances between the elements in the test structure were chosen such that the partial signals of interest, registered at ports 2 and 3, have identical propagation times. The wavelength of the input transducer is 1.6 μm ($p = 0.8$ μm), which corresponds to a center frequency close to 2.5 GHz on the 128° $LiNbO_3$ substrate.

There is one essential difference between the present case of a short reflector and the long reflectors studied previously [5]. For long reflectors, strong reflectivity is observed in the rather narrow frequency stopband of the reflector. Consequently, we used frequency-domain characteristics to determine the reflector parameters. For a short

grating, this approach does not work: the reflector properties are of wideband nature and the stopband is practically absent. Instead, we are obliged to estimate the reflectivity in the time domain. We used long (and, consequently, narrowband) pulses, and compared amplitudes of the incident and reflected pulses. For the estimation of energy losses, comparisons of frequency responses are used.

The bandwidth of an interdigital transducer, measured as the distance between the first zeros of the transfer function, can be estimated as:

$$\mathrm{BW_{IDT}} = \frac{2}{N_{\text{finger pairs}}}. \tag{1}$$

The frequency step Δf and simulation bandwidth B were set to 4 MHz and 2 GHz, thus yielding a 501-point frequency grid. In the time domain, according to:

$$\begin{aligned} T &= \frac{1}{\Delta f}, \\ \Delta t &= \frac{1}{\mathrm{B}}, \end{aligned} \tag{2}$$

the total time span T and the interval between time points Δt become 250 ns and 0.5 ns, respectively.

According to (1), a long transducer has a rather narrowband response. In the time domain, a reflected pulse is longer than the incident pulse due to the interaction with the reflector. If the reflector is short, the shape of the pulse is not appreciably changed: a short (wideband) reflector reflects nearly all the spectral components of a long (narrowband) pulse. For a longer incident pulse, the transition zones at which the pulse is entering and leaving the reflector (giving rise to a change in the shape of the pulse) are of lesser importance in the response. The shorter the reflector with respect to the transmitting transducer, the smaller the perturbation.

For a long incident pulse (a long transmitting transducer), the reflection coefficient is practically independent of the pulse duration. However, from the point of view of our numerical experiment in which the physics and geometry of the test structure is tailored to be as close as possible to a real experimental setup, very long pulses are not a practical approach. Furthermore, the shorter simulation time associated with a lower number of electrodes is an advantage.

In all cases studied in this paper, the reflector structure is significantly shorter than the transmitting transducer. Nevertheless, the interaction of the incident pulse with the 2- and 3-electrode reflectors results in a small but finite broadening of the pulse in space and time. The minor increase in the duration of the pulse implies that the maximum signal level of the reflected pulse slightly decreases. Thus we can expect that the reflection coefficient for the pulse, determined with this technique, will be slightly lower than the reflection coefficient evaluated at a single frequency point.

To describe the reflection of SAW, we use the fact that Y-parameters ($\mathrm{Y_{21}}$, $\mathrm{Y_{31}}$) are actually proportional to the currents generated in the interdigital transducers (IDTs) at ports 2 and 3 and, thus, proportional to the SAW amplitudes incident on the transducers. The time-gating procedure reviewed in Section III allows one to extract from $\mathrm{Y_{21}}$ the contribution of the direct (incident) wave and that of the wave reflected from the grating. Consequently, the method renders possible the comparison of different SAW amplitudes. Note that the receiving transducers at ports 2 and 3 have a split-finger geometry and are considered short circuited in the framework of the Y-parameters. Thus, they create a minimal perturbation for the waves passing through.

Due to the relatively low overall number of fingers, the rigorous FEM/BEM simulations of the test structures with short reflectors require a feasible execution time. With a 500 MHz computer, the simulation time for 501 frequency points for the test structure of Fig. 1 with two strips in the grating is roughly 3 hours.

III. FFT and Time Gating

Inverse Fourier transform is used for time gating. Typical time-domain representations of the signals for the test structure of Fig. 1, observed at ports 2 and 3, are shown in Fig. 2. Fig. 2(a) displays the absolute value of the time-domain representation of $\mathrm{Y_{21}}$, i.e., the signal transmitted from port 1 and received at port 2. The labeled peaks indicate the partial signals corresponding to the direct SAW propagation from port 1 to port 2 (signal α), and the propagation path to port 2, including a transmission through the receiving transducer at port 2 and a reflection from the reflector under study (signal β). Similarily, Fig. 2(b) illustrates the absolute value of the time-domain representation of $\mathrm{Y_{31}}$. The signal labeled γ is the direct partial signal and the one labeled δ is the signal reflected once from the grating and once from the transmitting transducer. In both figures, the vertical dashed lines indicate the truncation limits used in the time-gating procedure.

The source being in port 1, it is justified to assume that the admittances observed at ports 2 and 3 are—via the electric currents at ports 2 and 3 which they represent—proportional to the corresponding acoustic-wave amplitudes. The time-gating procedure allows one to extract from $\mathrm{Y_{21}}$ and $\mathrm{Y_{31}}$ the contributions of the direct (incident) waves ($\mathrm{Y_{21}^d}$, $\mathrm{Y_{31}^d}$) and from $\mathrm{Y_{21}}$ that of the wave reflected from the grating ($\mathrm{Y_{21}^r}$).

The short-circuited split-finger transducers at ports 2 and 3 give rise to a minimal perturbation for the waves passing through. However, in the case of small total reflectivity of the grating, the perturbation may have a visible effect on the analysis results. Thus, the direct signal registered at port 3, obtained from a simulation of the operation of a test structure without the reflector, $\mathrm{Y_{31}^{d,ref}}$, is used as the reference signal. Contrary to choosing $\mathrm{Y_{21}^d}$ as a reference, the scattering from the receiving split-finger transducer at port 2 then is eliminated. Note also that all the partial signals then have equal propagation distances.

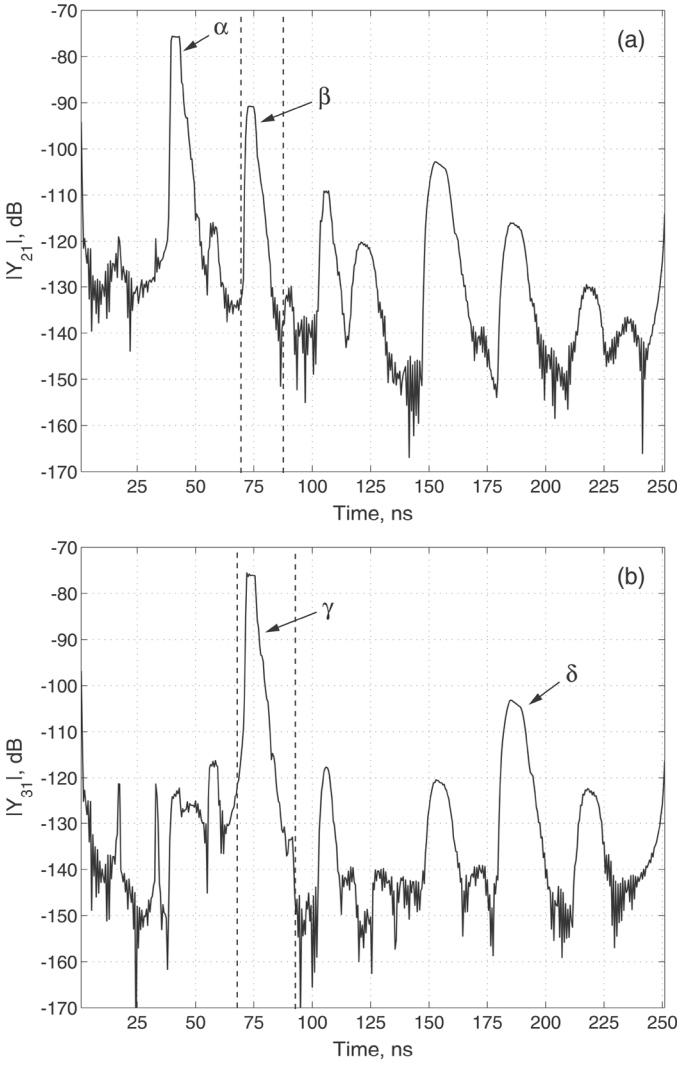

Fig. 2. Time-domain responses for the test structure in Fig. 1. (a) Signal transmitted from port 1 and received at port 2. The vertical dashed lines confine the contributions of the direct signal and the signal reflected once from the grating. See the text for the labels. (b) Signal transmitted from port 1 and received at port 3. The labels are dealt with in the text. Here, $a/p = 0.50$, $p = \lambda_0$, $h/\lambda_0 = 5\%$.

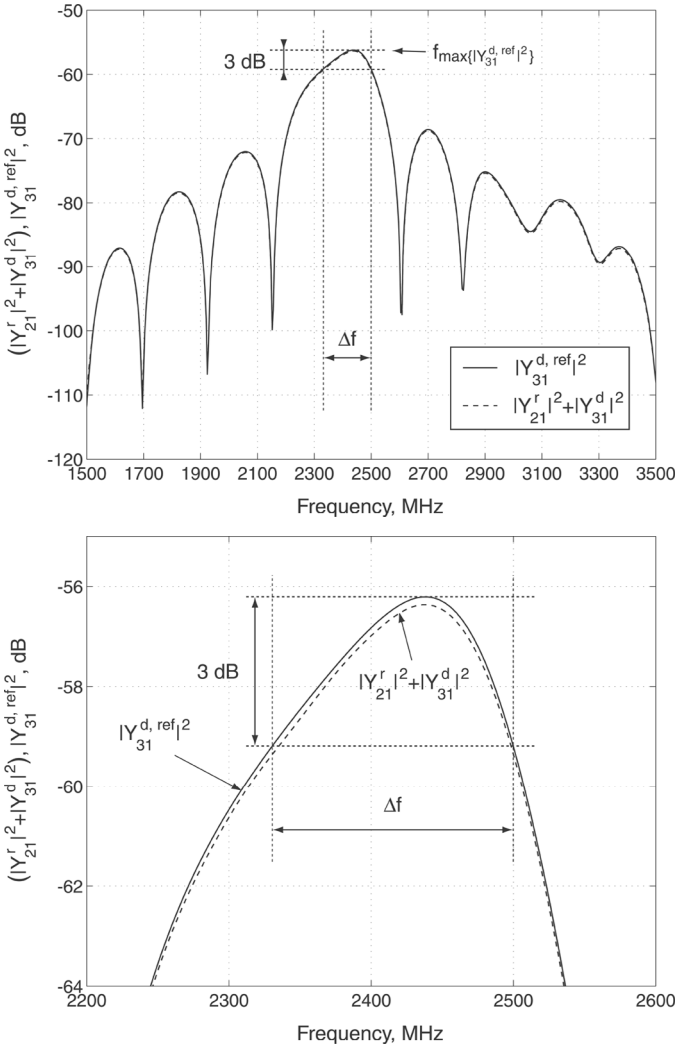

Fig. 3. Energy balance for the structure shown in Fig. 1. Above: Total calculated response. Below: Detailed view. The dashed vertical lines indicate the averaging regime for attenuation. Here, the reflector has two electrodes and the second-harmonic geometry ($p = \lambda_0$). The substrate is 128° YX-$LiNbO_3$ with $h/\lambda_0 = 5\%$ and metallization ratio $a/p = 0.50$.

Energy comparison serves as a method for evaluating the losses:

$$|\mathrm{Y}_{31}^{\mathrm{d,ref}}|^2 \geq |\mathrm{Y}_{21}^{\mathrm{r}}|^2 + |\mathrm{Y}_{31}^{\mathrm{d}}|^2, \tag{3}$$

where the superscripts d and r refer to the direct and reflected signals, respectively.

Green's functions describing the substrate properties conventionally involve the acoustic losses in the material. The FEM/BEM simulator used facilitates the inclusion of an intrinsic propagation loss and the resistivity of the electrodes. For short reflectors, however, the total reflectivity and attenuation attributed to the grating structure are substantially smaller than those for long reflectors, approaching the level of intrinsic losses. Consequently, in our calculations of the reflectivity and the attenuation due to scattering into the bulk, lossless Green's functions were used and resistivity excluded.

As far as the attenuation is concerned, the methodology used for long reflectors also was applied to short gratings. Because, due to the test structure geometry (see Fig. 1), the incident signal has a narrowband character, we can estimate the scattering losses of our reflector only in a relatively narrow frequency band close to the center frequency of the input transducer (see Fig. 3). The averaging band Δf was determined as the -3 dB bandwidth around the frequency where $|\mathrm{Y}_{31}^{\mathrm{d,ref}}|$ attains its maximum value. The amplitude attenuation value (in Nepers per wavelength) was obtained from the energy comparison of (3) by averaging over Δf:

$$\gamma\lambda_0 = \frac{1}{2\mathrm{L_g}} \cdot \mathrm{mean}\left\{ \ln\left(\frac{|\mathrm{Y}_{31}^{\mathrm{d,ref}}|^2}{|\mathrm{Y}_{21}^{\mathrm{r}}|^2 + |\mathrm{Y}_{31}^{\mathrm{d}}|^2} \right) \right\}_{\Delta f}, \tag{4}$$

where $\mathrm{L_g}$ is the length of the grating in wavelengths. For single-electrode reflectors, the attenuation was given per electrode (γ_{el}; $\mathrm{L_g} = 1$).

The extraction of the reflectivity for short grating structures calls forth an approach different from that applied to long reflectors [5]. As opposed to a long reflector, the total reflectivity of a grating consisting of only a few electrodes is too small and of too wideband a nature to produce a visible stopband notch in the frequency-domain response of the signal transmitted through the grating (Y_{31}^{d}). Instead, we can estimate the reflectivity in the time domain. A comparison of the levels of the reference signal ($|Y_{31}^{d,ref}(t)|$) and the signal reflected from the grating and registered at port 2 (reflected signal, $|Y_{21}^{r}(t)|$) in the time-domain representation of Y_{21}, gives an estimate for the reflectivity of short structures. Because the transmitted pulse has a definite duration due to the finite length of the transmitting transducer, the maximum values of the amplitudes of the direct and reflected signals were considered.

In what follows, the results of the simulations are interpreted in terms of reflectivity and attenuation per unit length, in a manner similar to the coupling-of-modes (COM) model terminology.

IV. Results

The rigorous FEM/BEM simulator [6] was applied to evaluate the reflectivity and the attenuation for Rayleigh waves on 128° YX-cut $LiNbO_3$ in short reflectors. The electrodes in the reflectors were grounded or open-circuited. The materials parameters by Kovacs *et al.* [7] were used, and the aluminum electrodes were assumed rectangular and isotropic. The results are presented as a function of the metallization ratio a/p (for the second harmonic grating, $a/p = a/\lambda_0$) and the relative electrode thickness h/λ_0.

A. Attenuation

The estimated attenuation resulting from the scattering into bulk waves, evaluated as a function of a/p and h/λ_0 for a single-electrode reflector, is presented in Fig. 4, and those obtained for 2- and 3-electrode gratings in Fig. 5 and Fig. 6. All values are in Nepers. For the single-electrode cases, the values are shown as such (per electrode). For the 2- and 3-electrode configurations, the values shown are normalized to the length of the grating in λ_0.

In all the figures, the attenuation increases as a function of h/λ_0. For the fundamental mode of operation ($p/\lambda_0 = 0.5$), the attenuation increases almost linearly with a/p. For a single-electrode case, the attenuation within a grounded electrode is slightly lower than that within a floating electrode, see Figs. 4(a) and (b). The termination condition has a similar but more pronounced influence on the 2- and 3-electrode gratings, compare Fig. 5(a) with 5(b) and Fig. 6(a) with 6(b). Although this difference is visible, it is not as large as expected [1].

For the second harmonic gratings ($p/\lambda_0 = 1.0$), the attenuation for small electrode thicknesses displays a saturation for increasing a/p, and for high electrode thicknesses it reaches a maximum then decreases with a/p. Note that

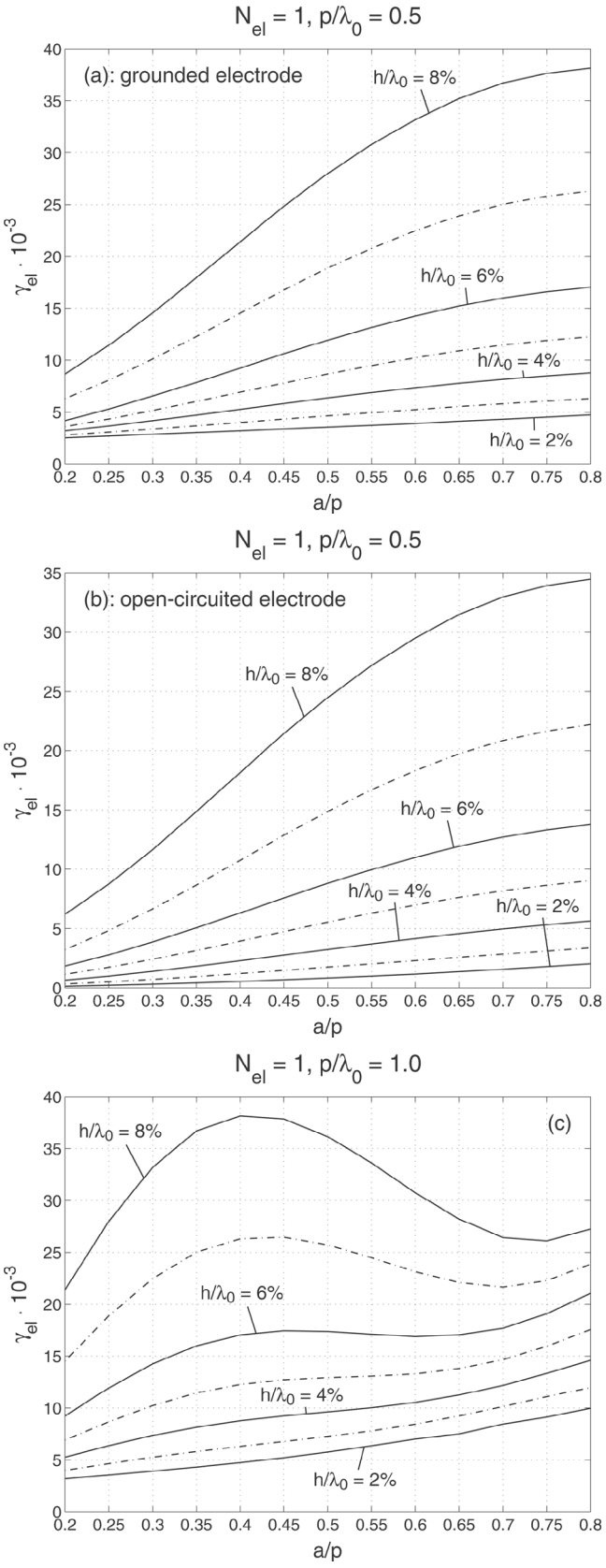

Fig. 4. Attenuation in Nepers for a single electrode as a function of a/p and h/λ_0. Note the overlap of the data sets. See the text for explanation. (a) Fundamental mode of operation ($p = \lambda_0/2$), grounded electrode. (b) Fundamental mode of operation ($p = \lambda_0/2$), floating electrode. (c) Second-harmonic mode ($p = \lambda_0$). The dash-dotted lines indicate the values for thicknesses 3, 5, and 7% of h/λ_0.

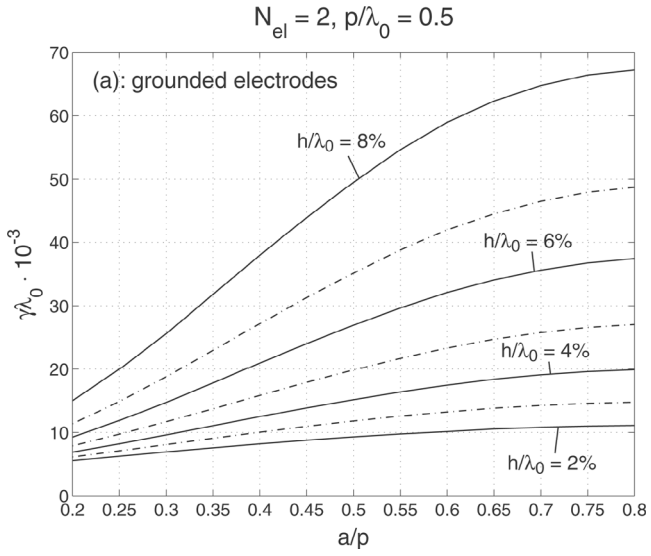

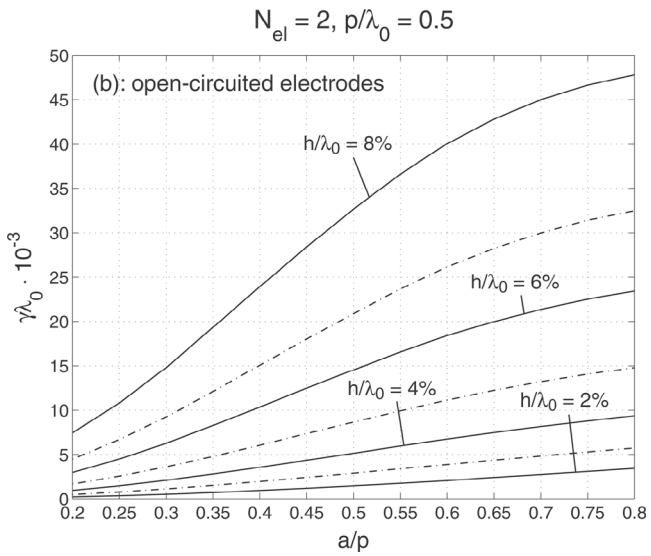

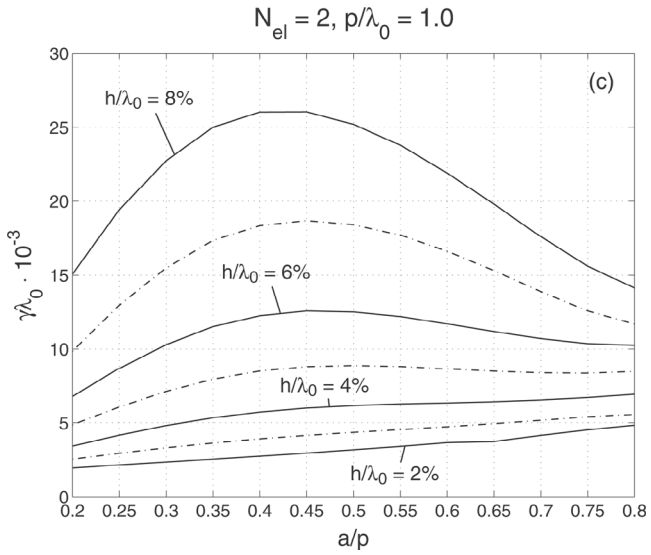

Fig. 5. Attenuation normalized to λ_0 in a 2-electrode grating as a function of a/p and h/λ_0. (a) Fundamental mode of operation ($p = \lambda_0/2$), grounded electrodes. (b) Fundamental mode of operation ($p = \lambda_0/2$), floating electrodes. (c) Second-harmonic mode ($p = \lambda_0$). The dash-dotted lines indicate the values for thicknesses 3, 5, and 7% of h/λ_0.

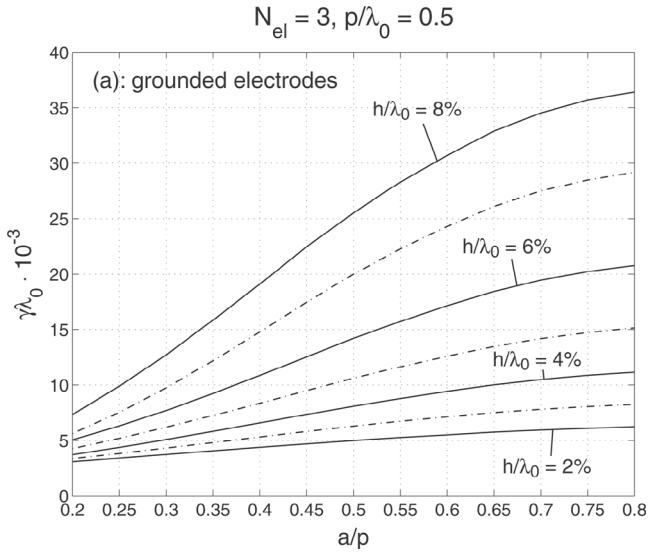

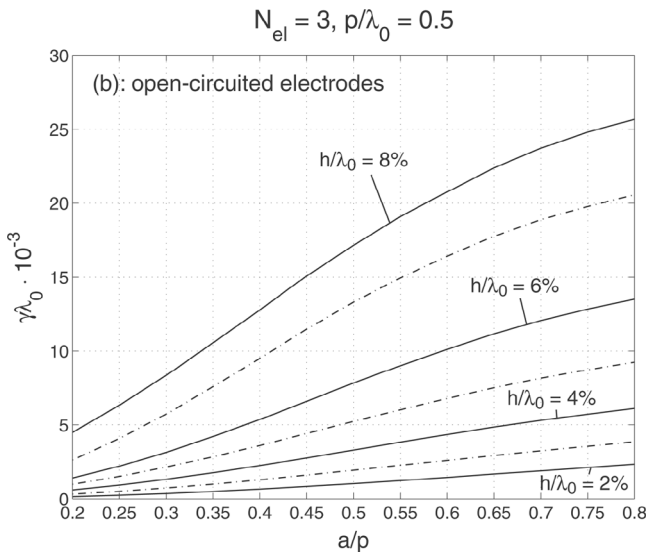

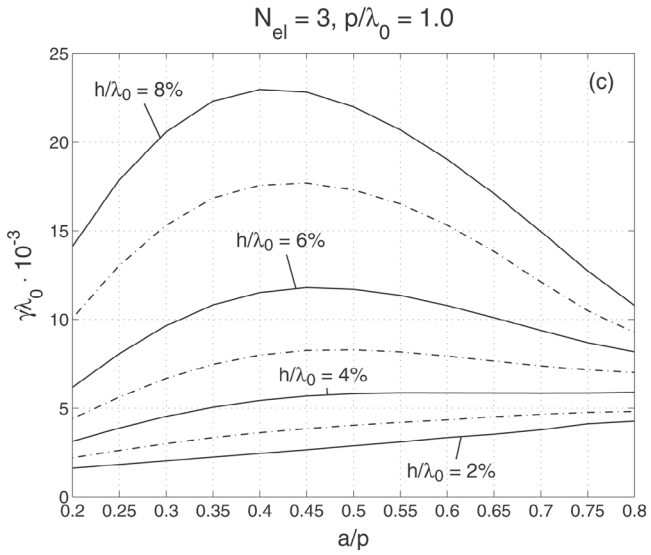

Fig. 6. Attenuation normalized to λ_0 in a 3-electrode grating as a function of a/p and h/λ_0. (a) Fundamental mode of operation ($p = \lambda_0/2$), grounded electrodes. (b) Fundamental mode of operation ($p = \lambda_0/2$), floating electrodes. (c) Second-harmonic mode ($p = \lambda_0$). The dash-dotted lines indicate the values for thicknesses 3, 5, and 7% of h/λ_0.

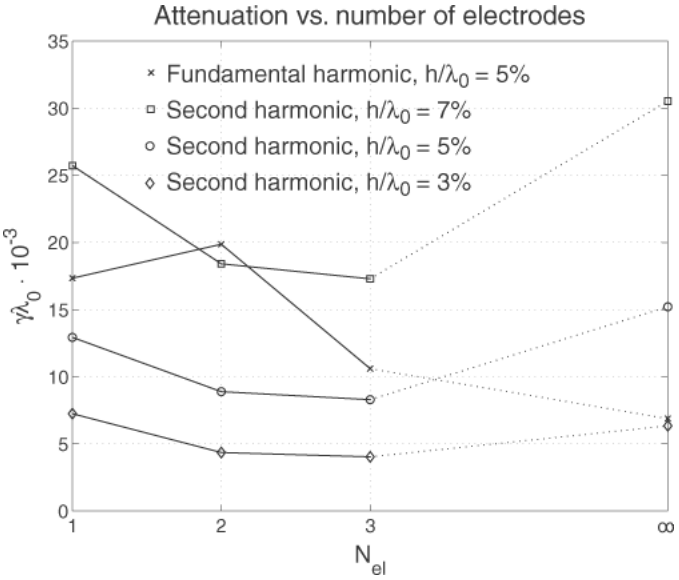

Fig. 7. Attenuation per wavelength as a function of number of electrodes. For the fundamental-mode, single-electrode case, the value for attenuation per electrode is multiplied by 2. The attenuation for long reflectors is taken from [5].

the attenuation in a single-electrode case [Fig. 4(c)] appears considerably larger than that for 2- and 3-electrode gratings, see Figs. 5(c) and 6(c).

Note also that, for the single-electrode case, the curves in Fig. 4(c) can be considered a continuation of those in Fig. 4(a). Actually, the characteristic length of a period cannot be defined for a single-electrode structure. The only available parameter for 1-electrode gratings is the width of the single electrode. For instance, the metallization ratio $a/p = 0.6$ in Fig. 4(a) corresponds to the metallization ratio $a/p = 0.3$ in Fig. 4(c). All the point pairs in these locations corresponding to equal electrode thicknesses thus have exactly the same values. Evidently, due to the different periodicities and normalization factors, a similar connection does not exist for the 2- or 3-electrode reflectors.

When the reflector grating comprises only a few electrodes, its reflecting and scattering properties may differ significantly from those of a long structure [1]. In addition to the contribution to the overall reflectivity, the periodicity affects the level of the energy scattered into the bulk. The bulk waves scattered from different electrodes interfere and, in certain directions, have opposite phases and cancel each other. Based on this reasoning, it is justified to assume that, for the fundamental mode of operation, the attenuation due to scattering, normalized to the length of the short reflector, decreases with the length of the grating.

Fig. 7 illustrates the attenuation versus the number of electrodes in the grating. For the purpose of comparison, the attenuation for the fundamental-mode, single-electrode reflector [Fig. 4(a), grating length taken here as $0.5\lambda_0$] is multiplied by two to have a value normalized to a wavelength. The entries for long gratings are the frequency-stopband values taken from [5].

The attenuation per wavelength tends to decrease with the increasing number of electrodes. The tendency is more pronounced for the fundamental-mode reflector, although the first point (single electrode, see Fig. 7) drops out from the curve. The comparison with earlier results shows that the attenuation values obtained in this work are of the same magnitude as those for long gratings [5]. However, a detailed comparison is hardly possible as long gratings exhibit a narrowband behavior and, consequently, different attenuation values were obtained for the grating stopband and for the passband.

B. Reflectivity

The reflectivity evaluated as a function of a/λ_0 and h/λ_0 for a single-electrode reflector is presented in Fig. 8 and those obtained for 2- and 3-electrode gratings in Figs. 9 and 10. For the single-electrode cases, the values shown are presented unnormalized, and for the 2- and 3-electrode structures they are normalized to the length of the grating in λ_0. See the guidelines of normalization in Section IV-A. Again it should be noted that the total lengths of the 2- and 3-electrode fundamental-mode gratings are taken to be λ_0 and $1.5\lambda_0$, respectively, as opposed to the lengths $2\lambda_0$ and $3\lambda_0$ for the 2- and 3-electrode second-harmonic gratings. Bearing this in mind, it is evident that for a/p up to 0.5 the reflectivity per electrode at the second harmonic frequency is considerably higher than that for the fundamental mode of operation. Note also that, as indicated in the context of attenuation (Section IV-A), the data sets for the grounded single-electrode fundamental-mode and second-harmonic mode reflector geometries partly overlap, see Figs. 8(a) and (c). The combination of a very weak reflectivity and a high metallization ratio ($a/p = 0.65 \ldots 0.75$), see, e.g., Fig. 8(c), appears to be beyond the application range of the extraction method used.

The reflectivity increases with increasing electrode thickness for all but a few simulated geometries. For the fundamental harmonic, see Figs. 8(a) and (b), 9(a) and (b), and 10(a) and (b), the increase in reflectivity as a function of a/p is close to linear. The 2- and 3-electrode thin grounded reflectors [Figs. 9(a) and 10(a)] display a minimum in the reflectivity, and such a phenomenon is not seen either in the open-circuited cases [Figs. 9(b) and 10(b)] or in the single-electrode responses [Figs. 8(a) and (b)]. Moreover, the reflectivities obtained for the open-circuited 2- and 3-electrode gratings [Figs. 9(b) and 10(b)] are notably higher than those obtained for the corresponding grounded geometries [Figs. 9(a) and 10(a)]. For the second harmonic mode, the reflectivity attains a maximum value for $a/p = 0.40$, then decreases for increasing a/p, see Figs. 8(c), 9(c) and 10(c).

Comparing the reflectivities of the 1–3-electrode fundamental-mode reflectors—see Figs. 8(a) and (b), 9(a) and (b), and 10(a) and (b), a slight decrease in reflectivity as a function of the grating length is observed. For comparison, some data points calculated for infinite periodic gratings are included in Figs. 10(a) and (b). The values for short-circuited gratings are obtained with a periodic

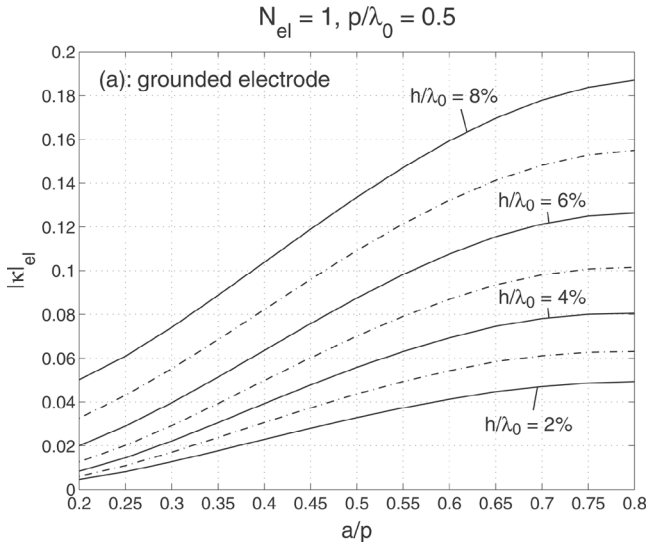

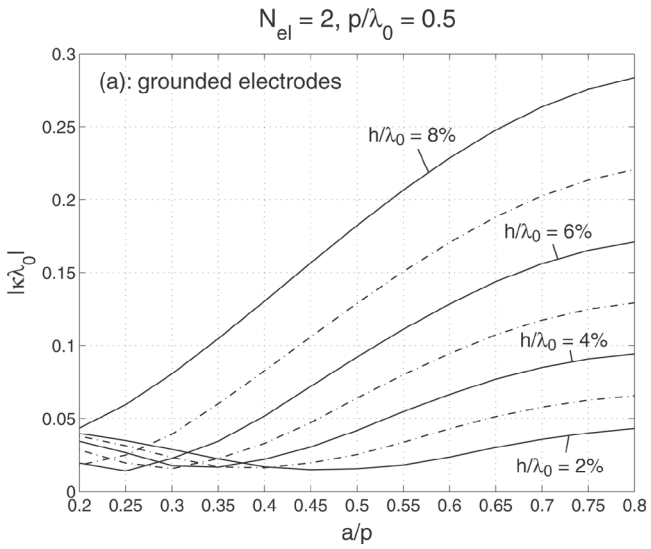

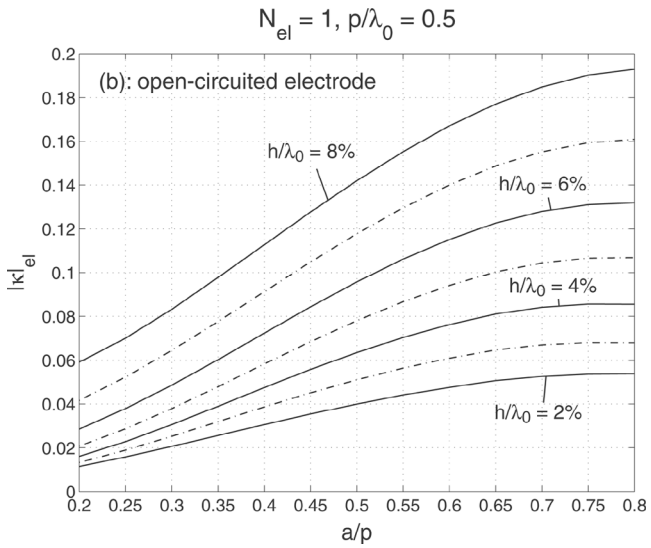

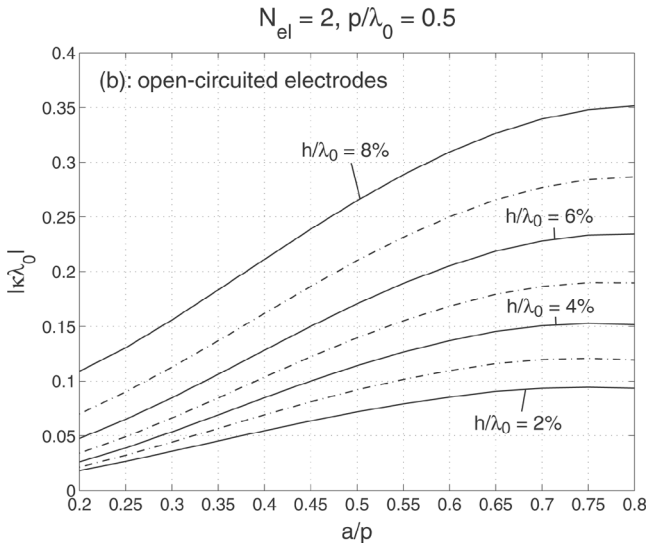

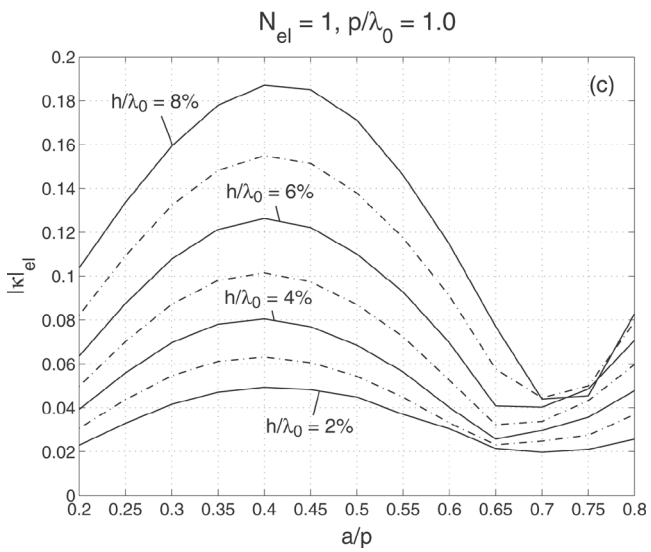

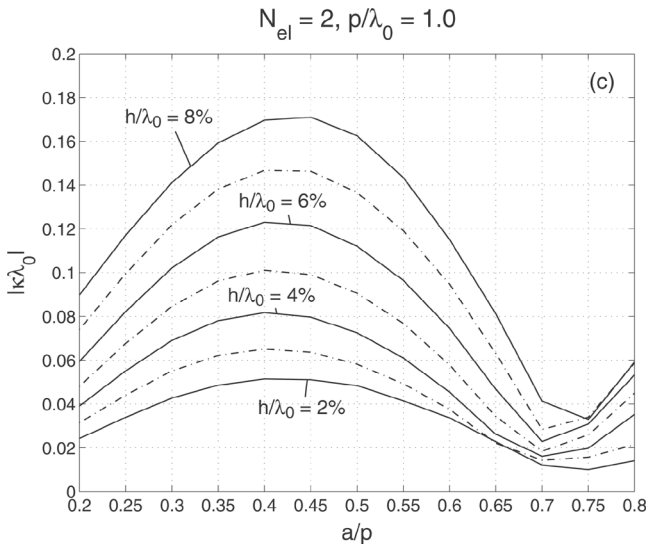

Fig. 8. Reflectivity for a single electrode as a function of a/p and h/λ_0. Note the overlap of the data sets. (a) Fundamental mode of operation ($p = \lambda_0/2$), grounded electrode. (b) Fundamental mode of operation ($p = \lambda_0/2$), floating electrode. (c) Second-harmonic mode ($p = \lambda_0$). The dash-dotted lines indicate the values for thicknesses 3, 5, and 7% of h/λ_0.

Fig. 9. Reflectivity normalized to λ_0 in a 2-electrode grating as a function of a/p and h/λ_0. (a) Fundamental mode of operation ($p = \lambda_0/2$), grounded electrodes. (b) Fundamental mode of operation ($p = \lambda_0/2$), floating electrodes. (c) Second-harmonic mode ($p = \lambda_0$). The dash-dotted lines indicate the values for thicknesses 3, 5, and 7% of h/λ_0.

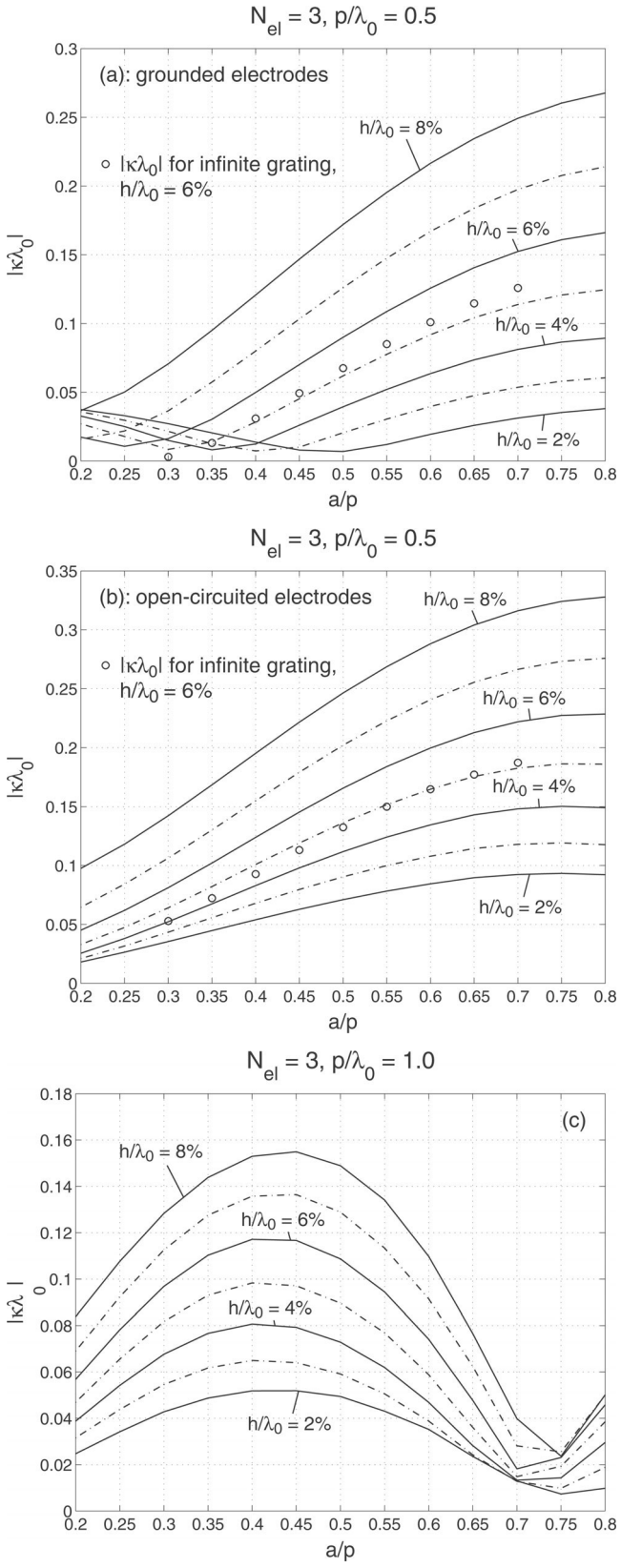

Fig. 10. Reflectivity normalized to λ_0 in a 3-electrode grating as a function of a/p and h/λ_0. (a) Fundamental mode of operation ($p = \lambda_0/2$), grounded electrodes. (b) Fundamental mode of operation ($p = \lambda_0/2$), floating electrodes. (c) Second-harmonic mode ($p = \lambda_0$). Circles denote values for infinite gratings with $h/\lambda_0 = 6\%$. The dash-dotted lines indicate the values for thicknesses 3, 5, and 7% of h/λ_0.

FEM/BEM simulator [8], and those for the open-circuited gratings are approximated using known relations.

Keeping the normalization convention in mind, one may take notice that the reflectivity per electrode for grounded gratings displays a notable decrease with the inclusion of the second electrode, see Figs. 8(a) and 9(a). A similar behavior is observed in a lesser extent for open-circuited gratings, see Figs. 8(b) and 9(b). For the single-electrode case, the difference between the two termination conditions studied is practically invisible, compare Figs. 8(a) and (b). The small difference observed is due to charges accumulated on the grounded electrode originating from the electrostatic coupling with the transducers situated far away.

The comparison of Figs. 8(c), 9(c), and 10(c) reveals that, for the second-harmonic 1–3-electrode reflectors, the reflectivities per wavelength, or—in this particular case—reflectivities per finger, slightly decrease with grating length. However, the values still remain considerably lower than those for long grounded gratings [5]. In order to find out whether the potentially excessive length of the incident pulse affects the results, the simulation was rerun for certain geometries with the number of the electrodes in the transmitting transducer halved. The resulting values exhibited small variations in the reflectivity and the attenuation (typically on the order of 1%), suggesting that the approach applied in this work yields results in a correct direction. For very long and strongly reflecting gratings, the notch in the transmission characteristic for the test structures used in [5], originating from the frequency stopband of the reflector, is so deep that its bottom is screened by the noise floor. This renders the precise evaluation of the reflectivity difficult.

V. Summary

We have numerically investigated short reflectors operating at the fundamental and second harmonic frequencies on 128° $LiNbO_3$. The results obtained from rigorous FEM/BEM simulations in this work suggest that practically feasible reflectivities can be achieved with reasonable electrode thicknesses. As a general rule, the reflectivity increases as a function of h/λ_0. The fundamental-mode gratings display a nearly linear increase in reflectivity with a/p, and the second-harmonic gratings—in particular for large electrode thicknesses—show a decrease in reflectivity after a maximum value at $a/p = 0.40 \ldots 0.45$. For the fundamental mode of operation, open-circuited gratings exhibit a notably higher reflectivity than the grounded reflectors.

According to our simulations, the losses due to bulk acoustic wave scattering inside the grating increase with increasing thickness of the aluminium electrodes. The attenuation behavior as a function of a/p closely resembles that of reflectivity: the fundamental-mode gratings exhibit a linear increase in losses and, for the second-harmonic gratings, the attenuation reaches a maximum for $a/p = 0.40 \ldots 0.45$.

Acknowledgments

The authors are grateful to Clinton Hartmann for useful discussions and to Natacha Béreux for generous help with simulations. This work was supported by Thales Microsonics SA (presently Temex Microsonics). The first author further acknowledges the Academy of Finland for support within the Graduate School in Technical Physics and the NOKIA Foundation and the Foundation of Technology (Finland) for scholarships. This work has been carried out in the framework of the Eureka project E! 2442 (New Surface Acoustic Wave Filter Generation for Mobile Telecommunications SUMO).

References

[1] S. V. Biryukov, Y. V. Gulyaev, V. V. Krylov, and V. P. Plessky, *Surface Acoustic Waves in Inhomogenous Media*. Berlin: Springer, 1995, pp. 324–326.

[2] L. Reindl and W. Ruile, "Programmable reflectors for SAW-ID-tags," in *Proc. IEEE Ultrason. Symp.*, 1993, pp. 125–130.

[3] F. Schmidt and G. Scholl, "Wireless SAW identification and sensor systems," in *Advances in Surface Acoustic Wave Technology, Systems and Applications*. vol. 2, C. C. W. Ruppel and T. A. Fjeldy, Eds. Singapore: World Scientific, 2001, pp. 227–326.

[4] S. Lehtonen, V. P. Plessky, and M. M. Salomaa, "Short reflectors operating at the fundamental and second harmonics on 128° $LiNbO_3$," in *Proc. IEEE Ultrason. Symp.*, 2002, pp. 321–325.

[5] S. Lehtonen, V. P. Plessky, J. Koskela, and M. M. Salomaa, "Second-harmonic reflectors on 128° $LiNbO_3$," *IEEE Trans. Ultrason., Ferroelect., Freq. Contr.*, vol. 50, pp. 972–978, Aug. 2003.

[6] P. Ventura, J. M. Hodé, M. Solal, J. Desbois, and J. Ribbe, "Numerical methods for SAW propagation characterization," in *Proc. IEEE Ultrason. Symp.*, 1998, pp. 175–186.

[7] G. Kovacs, M. Anhorn, H. E. Engan, G. Visintini, and C. C. W. Ruppel, "Improved material constants for $LiNbO_3$ and $LiTaO_3$," in *Proc. IEEE Ultrason. Symp.*, 1990, pp. 435–438.

[8] J. Koskela, V. P. Plessky, and M. M. Salomaa, "SAW/LSAW COM parameter extraction from computer experiments with harmonic admittance of a periodic array of electrodes," *IEEE Trans. Ultrason., Ferroelect., Freq. Contr.*, vol. 47, pp. 806–816, 1999.

Saku Lehtonen received the M.Sc. degree in technical physics from Helsinki University of Technology (HUT) in 1998. He is a postgraduate student in the Materials Physics Laboratory at HUT.

His research interests include high-frequency SAW devices and characterization of SAW grating structures.

Victor P. Plessky (M'93–SM'01) received his Ph.D. degree in physical and mathematical sciences at the Moscow Physical-Technical Institute and the Dr.Sc. degree at the Institute of Radio Engineering and Electronics (IRE, Russian Academy of Sciences, Moscow), in 1978 and 1987, respectively. Beginning in 1978, he worked at IRE, first as a junior researcher, and, in 1987, he was promoted to the position of Laboratory Director. In 1991, he also worked as a part-time professor at the Patris Lumumba University, Moscow. He received the full professor title in 1995 from the Russian Government.

In 1992, he joined ASCOM Microsystems SA in Bevaix, Switzerland, where he worked as a special SAW projects manager. Since 1997, he has lectured several courses on various SAW topics at Helsinki University of Technology as a visiting professor. Since 1998 he has been working at the Neuchâtel, Switzerland office of Thomson Microsonics (later Thales Microsonics, presently Temex Microsonics), from 2002 as a consultant. He has been engaged in research on semiconductor physics, SAW physics (new types of waves, scattering and reflection on surface irregularities, laser generation of SAW), SAW device development (filters, delay lines, reflective array compressors), and magnetostatic wave studies.

His current interests focus on SAW physics and low-loss SAW filter development. Professor Plessky is an IEEE Senior Member. He was awarded the USSR National Award for Young Scientists in 1984.

Martti M. Salomaa (M'95) received his Dr.Tech. degree in technical physics from Helsinki University of Technology (HUT) in 1979. Thereafter, he worked at University of California, Los Angeles (UCLA) and the University of Virginia, Charlottesville, VA. From 1982 to 1991, he was the theory group leader at the Low Temperature Laboratory, HUT, and from 1988 to 1991, he served as the director of the ROTA project between the Academy of Finland and the Soviet Academy of Sciences. He has held a sabbatical stipend at the University of Karlsruhe, Karlsruhe, Germany, and, in 1994, he was a guest professor at ETH-Zürich. Since 1996, he has been a professor of technical physics and the Director of the Materials Physics Laboratory, Department of Engineering Physics and Mathematics, HUT.

He is a corecipient of the 1987 Award for the Advancement of European Science (presented by the Körber Foundation, Hamburg). His research interests include Bose-Einstein condensation, superfluidity, superconductivity, magnetism, physics of SAW, nondiffracting waves, nanoelectronics, mesoscopic physics, and sonoluminescence. He is a member of the IEEE, the American Physical Society, the European Physical Society, and the Finnish Physical and Optical Societies.